Materials and Design 65 (2015) 17–23

Contents lists available at ScienceDirect

Materials and Design

journal homepage: www.elsevier.com/locate/matdes

Interface microstructural control by probe length adjustment in friction stir welding of titanium and steel lap joint

Y. Gao [a,*], K. Nakata [a], K. Nagatsuka [a], F.C. Liu [a], J. Liao [b]

[a] Joining and Welding Research Institute, Osaka University, Ibaraki 567-0047, Japan
[b] Kurimoto Ltd., 2-8-45 Suminoe, Osaka 559-0021, Japan

ARTICLE INFO

Article history:
Received 20 June 2014
Accepted 12 August 2014
Available online 6 September 2014

Keywords:
Friction stir welding
Titanium
Steel
Intermetallic compound

ABSTRACT

The dissimilar lap joining of commercially pure Ti (CP-Ti) plate of 1.0 mm in thickness and structural steel (SPCC) plate of 3.2 mm in thickness was conducted by friction stir welding using different tools with probe lengths from 0.8 to 1.2 mm for the purpose of controlling the joint interface microstructure. The sound joints showing the base plate fracture of CP-Ti have been obtained by using the tools with the probe lengths of 0.9 and 1.0 mm. The transmission electron microscope examination revealed the two types of the interface microstructure. One was a non-intermixed type interface with a single interlayer of about 50–100 nm in thickness, composed of FeTi intermetallic compound and β-Ti phase at the joint with the probe length of 0.9 mm. The other was an intermixed interface with lamellar structure in which a FeTi or FeTi + Fe_2Ti intermetallic compound layer of about 100 nm in thickness and a β-Ti layer of about 1 μm in thickness were alternately formed at the joint with the probe length of 1.0 mm.

1. Introduction

Ti and its alloys exhibited excellent integrate performance such as high specific strength, considerable good high temperature mechanical properties and excellent corrosion resistance, thus have been applied in aerospace, transportation, power generation and chemical industries. However, a wider utilization of these materials is limited by their higher materials cost than conventional structural steels. One solution is to reduce the usage of Ti alloys by applying them selectively only to the required places, and in the other places steels should be applied instead of Ti alloys. To realize this, the Ti alloys need to be tightly joined to steels using a proper joining method.

The major metallurgical problem in joining Ti alloys with steels is the formation of brittle intermetallic compound phases, such as FeTi and/or Fe_2Ti, as indicated in Fig. 1 [1], which make the Ti alloys and steel hardly to be directly joined by conventional welding methods. To solve this problem, many welding and joining processes have been tried in recent years, such as electron beam welding [2–4], laser welding [5–6], explosive welding [7–8], diffusion welding [9–11], inertia friction welding [12–14] and friction stir welding (FSW) [15–17]. All these techniques for the Ti/steel dissimilar joint are still in the developmental stage and have their own insurmountable disadvantages. For example, fusion welding is not recommended because it usually associated with high heat input and the formation of massive brittle intermetallic compounds which will deteriorate the mechanical properties of the joints [3]. The major disadvantage of this explosive welding is that an expansive knowledge of explosives is needed before the procedure may be attempted. Explosion welding is therefore difficult to use broadly in the industry. On the other hand, during the diffusion bonding process, the whole metallic materials of the specimens needed to be heated to very high temperatures, and the diffusion process needs a long processing time to implement, which is not permitted in many industry applications. For the inertia friction welding, the samples can only be club-shaped and need the post-weld heat treatment to increase the bend ductility. The resultant conditions make the inertia friction welding difficult to apply.

FSW, a novel solid-state welding process developed by The Welding Institute (TWI), has several advantages such as a high operative efficiency and versatility as compared to the conventional solid-state welding processes. A preliminary investigation [15] showed that sound dissimilar lap joints of CP-Ti and 304 stainless steel through FSW have been achieved by adjusting tool rotation rate and welding speed under protecting atmosphere. On the other hand, Liao et al. have examined the interface microstructure of the FSW lap joint of CP-Ti and steel [16]. Swirling like macro-and micro-intermixing zones were formed at the joint interface. However, a detail investigation on the FSW of Ti to steel is still lacking

* Corresponding author. Tel./fax: +81 0668798668.
E-mail address: gaoyefei@jwri.osaka-u.ac.jp (Y. Gao).

http://dx.doi.org/10.1016/j.matdes.2014.08.063
0261-3069/

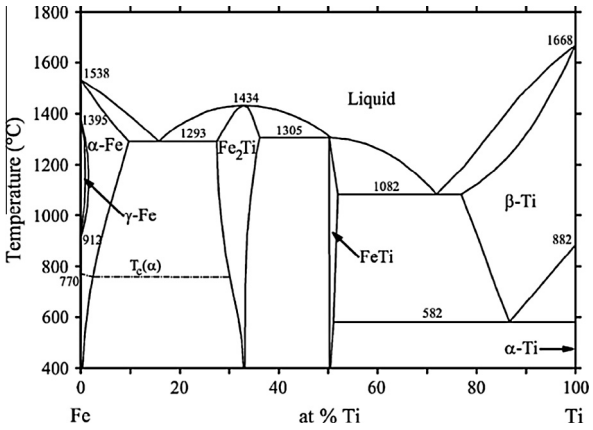

Fig. 1. Ti–Fe binary phase diagram.

and the joining mechanism of the dissimilar lap joint was still far from fully understand. In our preliminary work, the effect of tool rotation rate and welding speed on the microstructural evolution and mechanical properties of dissimilar FSW lap joint of CP-Ti and steel has been clarified [18]. Beside the tool rotation rate and welding speed, the probe length is also an important crucial parameter for the FSW lap welding of CP-Ti to steel, because it has a great influence on the interface microstructure, especially on the formation of intermetallic compound layer at the joint interface. Therefore, in present work, the effect of probe length on the interface microstructure was investigated to evaluate the morphology and the phase identification. The joining mechanism of CP-Ti to steel was determined through the transmission electron microscopy (TEM) observation on the two typical joint interface microstructures formed through adjusting the probe length of the FSW tool.

2. Experimental details

Plates of CP-Ti ($1 \times 85 \times 200\ mm^3$) and low carbon cold-rolled structural steel (SPCC, $3.2 \times 85 \times 200\ mm^3$) were subjected to FSW, and the CP-Ti was placed as a top plate and SPCC as a substrate plate (Fig. 2). Tables 1 and 2 show the nominal chemical compositions of the materials. The WC-Co based FSW tools consisted of a concave shoulder of 15 mm in diameter, a cylinder

Table 1
Nominal chemical composition of CP-Ti (mass.%).

Element	C	H	O	N	Fe	Ti
Mass.%	0.01	0.001	0.09	0.00	0.03	Balance

Table 2
Nominal chemical composition of SPCC (mass.%).

Element	C	Si	Mn	P	S	Fe
Mass.%	0.04	0.01	0.18	0.01	0.01	Balance

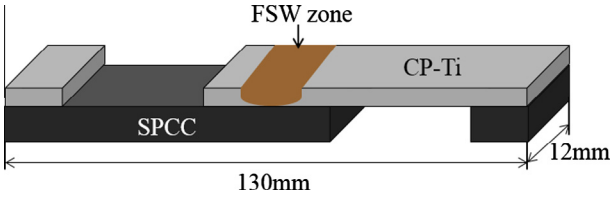

Fig. 3. Specimen for the tensile test.

probe of 6 mm in diameter but with variant probe lengths of 0.8, 0.9, 1.0, 1.1 and 1.2 mm, respectively, were used. Lap joining was performed at a tool rotation rate of 400 rpm, a welding speed of 50 mm/min and a load of 7.35 kN with a tool title angle of 3°.

The FSW joints were cross sectioned perpendicular to the welding direction for the metallographic analysis and tensile shear test using an electrical-discharge cutting machine. The specimens for optical microscopy were polished and then etched with an acid solution of 3 mL HF, 3 mL HNO_3 and 50 mL H_2O. Microstructure was studied using optical microscope (OM), scanning electron microscope (SEM) and TEM. The microhardness profile measurement was conducted on the cross-section of the lap joints using a microvickers hardness tester under a load of 0.98 N and a holding time of 15 s. Element distributions and chemical compositions of the joint interface were analyzed with an energy-dispersive X-ray spectrometer equipped with the TEM. In addition, shear tensile test was performed at room temperature with a constant cross-head speed of 1 mm/min by using three tensile specimens with a width of 12 mm for each joint. The configuration of the tensile specimens were set according to JIS Z 3136:1999 as shown in Fig. 3 [19].

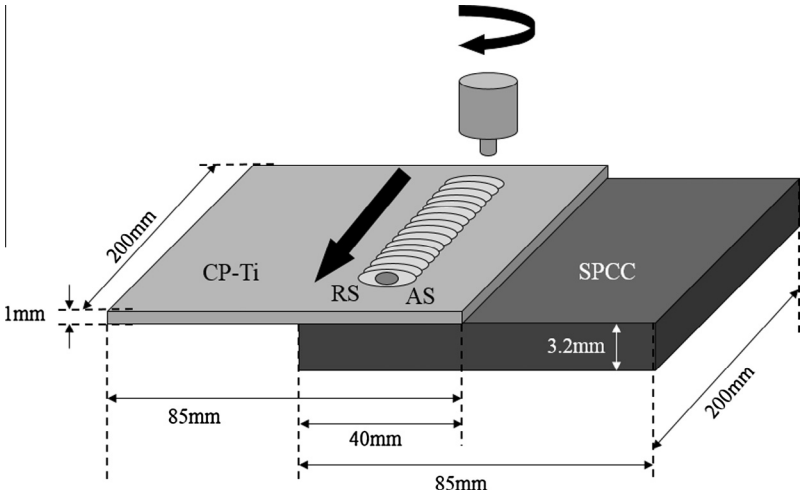

Fig. 2. Schematic diagram of the geometry of a dissimilar CP-Ti/SPCC lap design.

Table 3
Condition of the lap joints of CP-Ti and SPCC with same welding parameter but different probe lengths.

Probe length (mm)	Lap joint condition
0.8	Lap joint was not formed
0.9	Good lap joint
1.0	Good lap joint
1.1	Over heat, Ti coating to the tool
1.2	Over heat, Ti coating to the tool

3. Results and discussion

Table 3 summarizes the resultant conditions of the joints welded with the same welding parameters but different probe lengths. The welded joint with the probe length of 0.8 mm was not formed because the probe is too short, leading to insufficient plastic flow of CP-Ti at the interface. The sound welded joints were obtained when welded using the probes with length of 0.9 and 1.0 mm. The lap joints produced using probes with length of 1.1 and 1.2 mm exhibited the rough surface appearance because of the severe adhesion of Ti to the tool as shown in Fig. 4, which shows the appearances of the tool before and after FSW with the probe length of 1.1 mm. This is a common phenomenon observed with overheating condition for the FSW of Ti alloys [16].

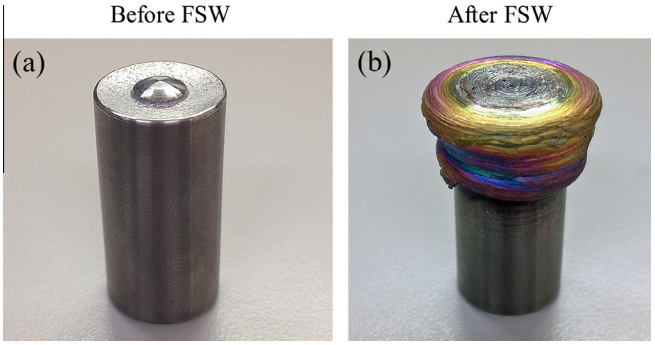

Fig. 4. Appearances of FSW tool, (a) before and (b) after FSW.

Fig. 5 shows the macrostructures (OM) and the three kinds of typical interfaces (SEM) in the cross-section of the joints, which were produced with the same FSW parameters but different probe lengths. The joint welded with the probe length of 0.9 mm showed a waved and simple interface, and no obvious intermixed zone was observed as shown in Fig. 5(a) and (d). The waved interface was formed by the direct contact between the probe tip and SPCC surface during welding. On the contrary, the joint welded with the probe length of 1.0 mm showed a dark colored intermediate zone at the interface between the SZ of CP-Ti and SPCC as typically shown in Fig. 5(b), which was revealed to be a lamellar structure, composed of CP-Ti and steel layers by the higher magnified SEM examination (Fig. 5(e)). The formation of such a microstructure can be attributed to the intensive intermixture of CP-Ti and SPCC induced by the enough long rotating probe to severe contact with SPCC surface. Fig. 5(c) shows the macrostructure (OM) of the interface of the joint welded with probe length of 1.1 mm. A large surface groove was formed because of severe adhesion of Ti to the tool as shown in Fig. 4. The joint welded with probe length of 1.2 mm got the similar surface and more worse. The joints welded with

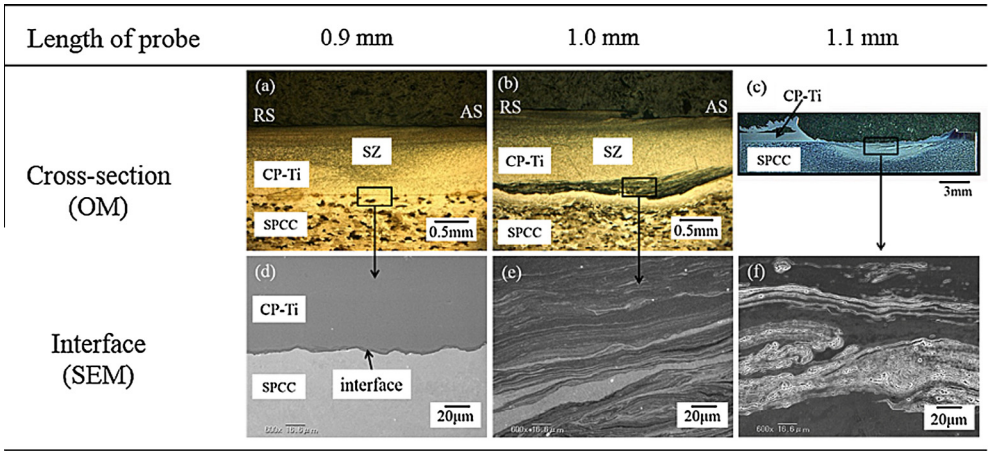

Fig. 5. Cross-sections and interfaces of the joints with constant welding parameters but different probe lengths.

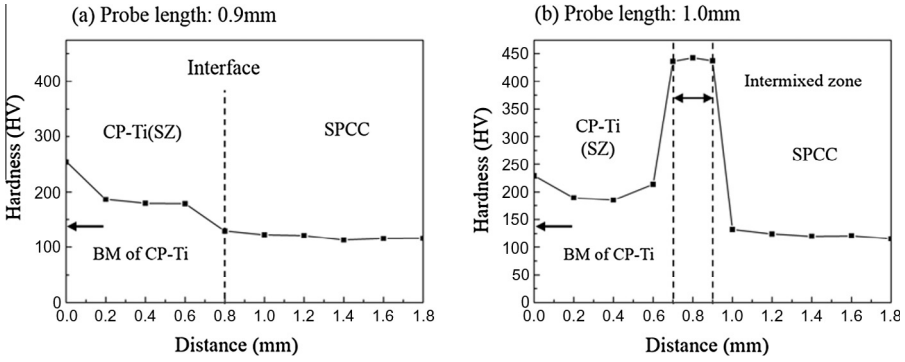

Fig. 6. Typical hardness profiles on the cross section of the lap joint welded with different probe lengths, (a) 0.9 mm and (b) 1.0 mm.

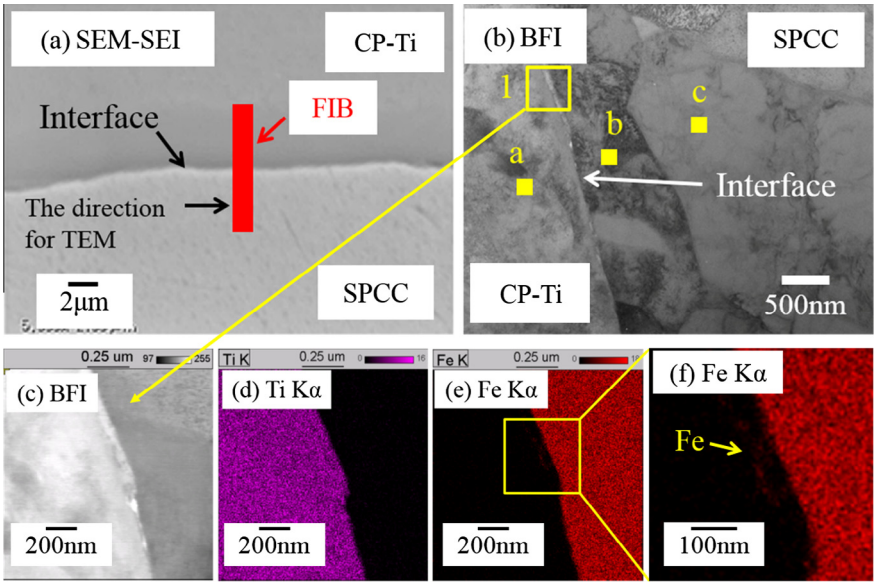

Fig. 7. The distribution of element of the non-intermixed interface, (a) SEM micro graph of the non-intermixed interface and (b) the TEM bright field image of the interface and (c) the higher magnified TEM bright field image and (d) Ti (e) Fe area maps, respectively and (f) the higher magnified Fe area map.

Table 4
Elemental analysis results at the positions a, b and c in Fig. 7(b).

Position	Element (at.%)		Phase
	Ti	Fe	
a	97.8	2.2	α-Ti
b	1.8	98.3	α-Fe
c	1.4	98.6	α-Fe

probe length 1.1 and 1.2 mm got more thermal input, because of the longer probes inserted into the steel and both of CP-Ti and steel were stirred during the FSW processing.

Fig. 6(a) and (b) show the micro-hardness profiles obtained on the cross-section of the two typical lap joints produced by the tools with probe lengths of 0.9 and 1.0 mm, respectively. The hardness in the SZ is higher than that in CP-Ti base metal (143 *HV*) in each case due to the grain refinement in SZ as well-demonstrated [20]. The intermixed interface in the joint produced by the tool with probe length of 1.0 mm (Fig. 6(b)) showed much higher hardness than both the SZ and the SPCC substrate, which suggested the formation of Fe–Ti intermetallic compounds in the intermixed interface region. However, no hardness peak was observed at the non-intermixed interface of the joint produced by the tool with probe length of 0.9 mm as shown in Fig. 6(a).

In order to clarify the formation mechanism of the wave and simple (non-intermixed) interface between CP-Ti and steel, the TEM sample across the joint interface was prepared by a focused ion beam (FIB) instrument as shown in Fig. 7(a) for the interface

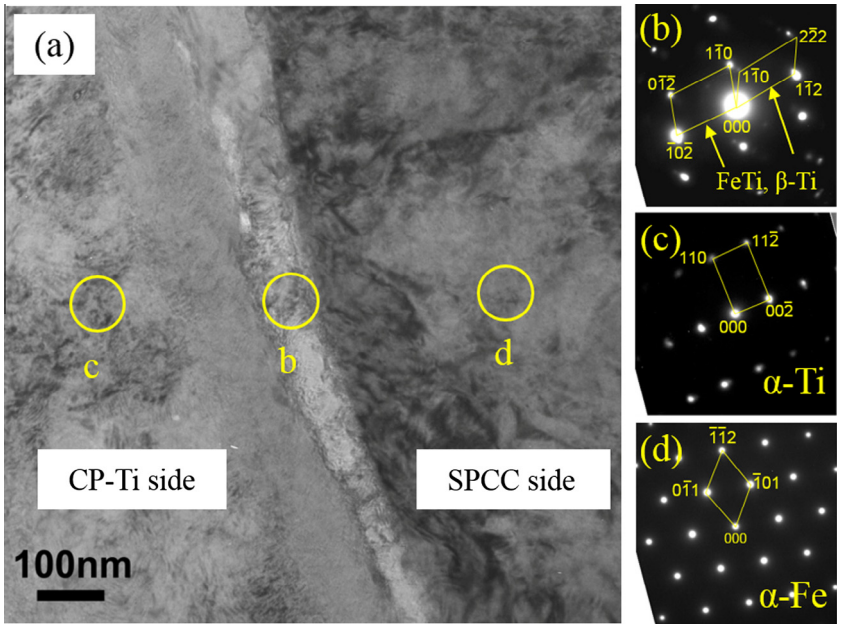

Fig. 8. TEM bright field image of the non-intermixed interface. (a) TEM bright field image of non-intermixed interface, (b) selected area diffraction pattern of the position b, (c) selected area diffraction pattern of the position c and (d) selected area diffraction pattern of the region d.

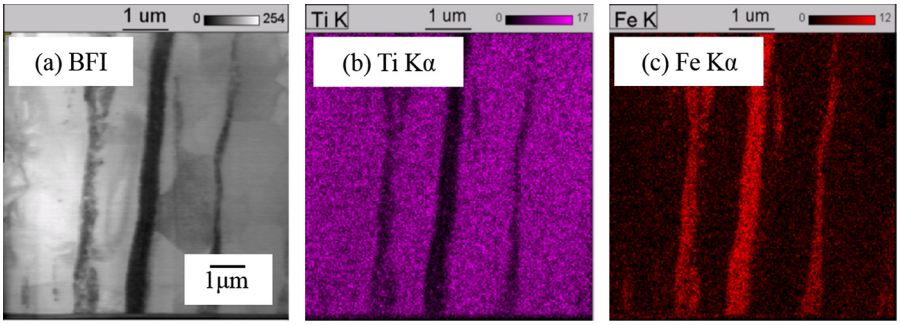

Fig. 9. The distribution of element of the intermixed interface, (a) the TEM bright field image of the interface and (b) the higher magnified TEM bright field image and (c) Ti (d) Fe area maps, respectively.

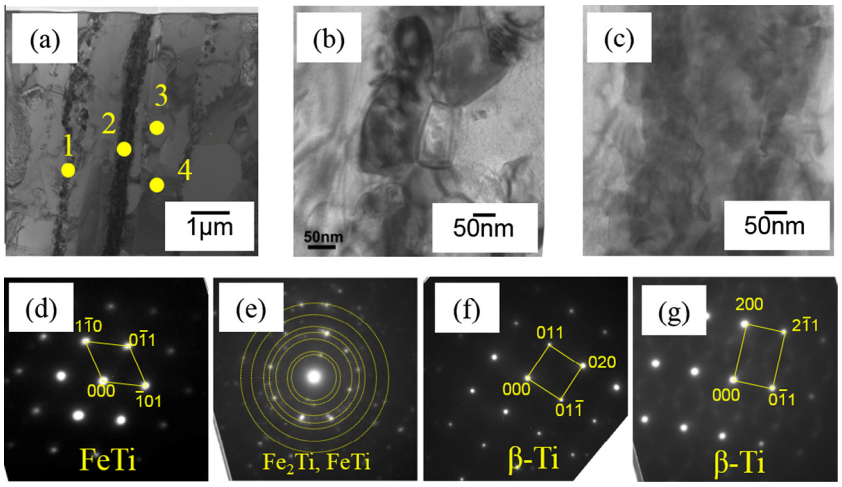

Fig. 10. TEM bright field image of the intermixed interface (a) and higher magnification images of position 1 (b) and position 2 (c). Selected area diffraction patterns of positions 1–4 in (a) are shown in (d)–(g), respectively.

analyzed by TEM and EDX. Fig. 7(b) shows that three different regions a, b and c were observed on the non-intermixed interface. According to the EDX elemental analysis as shown in Table 4, Region a was α-Ti phase containing a small amount of Fe, and Regions b and c were α-Fe phase with a small amount of Ti. According to these results, the location of the joint interface was confirmed to be between regions a and b, and very thin white interlayer was observed there as shown in Fig. 7(c), which is a higher magnification TEM micrograph of the square position 1 in Fig. 7(b). The distributions of Ti and Fe elements in the position 1 as shown in Fig. 7(d)–(f) indicate that the white interlayer was mainly composed of Ti, but some iron was also contained as observed in (f). Fig. 8(a) shows more higher magnification TEM micrograph of (c) in Fig. 7, and Fig. 8(b)–(d) show selected area diffraction patterns obtained from circular position b in this white interlayer, circular position c in the adjacent areas of CP-Ti side and circular position d in SPCC side, respectively. The thin white interlayer was revealed to be a composite layer of an intermetallic compound FeTi and β-Ti as identified in (b), though more detail morphology in the layer was not clear. The adjacent areas in CP-Ti and SPCC sides were identified to be α-Ti in (c) and α-Fe in (d) as each base material.

On the contrary, Fig. 9(a)–(c) show the TEM bright field image (BFI) of the typical microstructure of the intermixed interface and the distributions of Ti and Fe elements, respectively. These results made clear that the intermixed interface was composed of lamellar type microstructure, in which the dark thin layers observed in (a) were Fe-rich layer, and sandwiched by the Ti-rich layers. Fig. 10(b) and (c) shows the high magnification TEM micrographs of Fe-rich layer as shown by the positions 1 and 2 in Fig. 10(a), respectively and these dark zones corresponds to the Fe-rich layer according to the EDX result as shown in Fig. 9.

Table 5
Diffusion coefficients of Ti and Fe in α-Fe, α-Ti and β-Ti at 1155 K.

Matrix	Diffuse element	D ($m^2\ s^{-1}$)	D_0 ($m^2\ s^{-1}$)	Q (kJ mol^{-1})
α-Fe	Ti	1.07×10^{-14}	6.8×10^{-3}	261
α-Ti	Fe	1.27×10^{-13}	1.2×10^{-8}	110
β-Ti	Fe	1.60×10^{-12}	8.0×10^{-7}	126

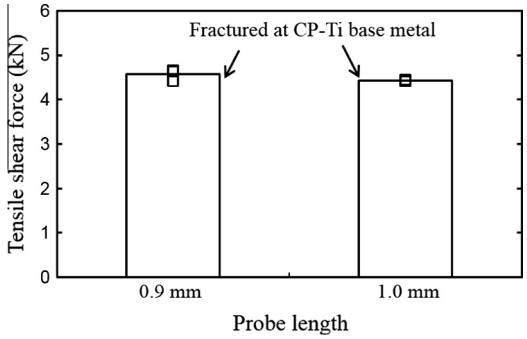

Fig. 11. Tensile shear force of the lap joints of CP-Ti and SPCC with constant welding parameter but different probe lengths.

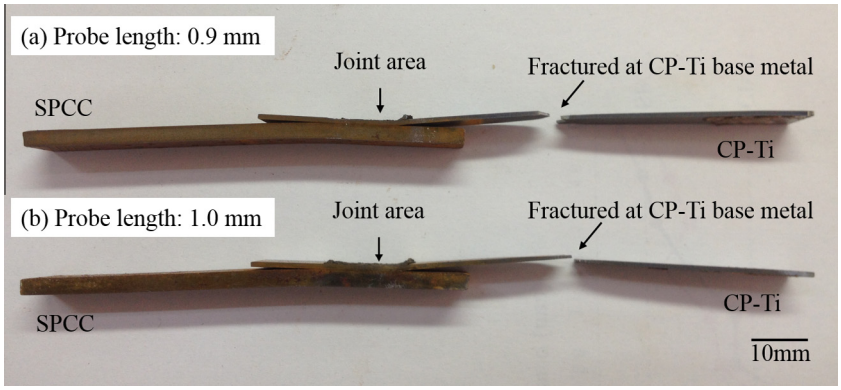

Fig. 12. Side view appearances of the lap joints welded with different probe lengths, showing the fracture location after shear tensile test.

Fig. 10(d)–(g) shows the selected area diffraction patterns of the positions 1, 2, 3 and 4, respectively in Fig. 10(a). Fe–Ti intermetallic compounds as FeTi and/or Fe_2Ti were identified at the Fe-rich layers (positions 1 and 2). On the contrary, Fe-Ti intermetallic compound was not detected at the Ti-rich layers (positions 3 and 4), and instead of this, β-Ti phase was identified, but α-Ti phase as the base material was not detected.

The β-Ti phase was found even at the ambient temperature together with Fe-Ti intermetallics (FeTi and Fe_2Ti) at these two typical kinds of the interface, the waved and simple-type non-intermixed and the lamellar-type intermixed interfaces. According to the binary Fe–Ti phase diagram [1], the β transus of Ti decreases with increasing Fe content from 1155 K to 855 K at the eutectoid reaction between Ti and FeTi. Therefore, it is possible that the temperature at the joint interface is above the β transus of Ti (1155 K), and β-Ti phase appears at the interface at the elevated temperature during FSW, and then, since the cooling rate at the stir zone, particularly at the interfacial zone of dissimilar joint is tremendously high [21], non-equilibrium phases are easily generated in FSW joint [22]. In addition, Fe is the strong β-Ti phase stabilizers [23] and the β-Ti phase contained Fe as shown in Fig. 9(c). As a result, it is considered that from these reasons, the β-Ti phase remained at the ambient temperature in the interfacial zones.

In present study, because of the very thin interlayer at the non-intermixed interface between CP-Ti and SPCC, the hardness of this layer cannot be detected by the micro-hardness measurement as shown in Fig. 8(a).

On the other hand, in the intermixed interface, β-Ti layer and Fe-rich layer are alternately formed in the wide range. As to the formation mechanism, it is considered that at first, a part of steel was stirred into CP-Ti as thin layers by a rotating probe and formed the lamellar-type intermixed interface during the FSW process as shown in Fig. 5(d). Then, since small solubility of Ti in the solid solution of iron even at the elevated temperature, FeTi and/or Fe_2Ti were easy to form in the Fe-rich zone (positions 1 and 2) by the diffusion reaction, though these intermetallic compounds were not found in the Ti-rich zone (positions 3 and 4), and which was consisted of β-Ti phase at the intermixed interface as shown in Fig. 10(a).

The diffusions of Ti and Fe are very important for the lap joint formation between CP-Ti and SPCC. According to Fick's first law of diffusion, the diffusion coefficient D is an important physical quantity, and diffusion coefficient D is

$$D = D_0 \exp(-Q/RT) \quad (1)$$

where D_0 is the diffusion constant, Q is the activation energy of diffusion, R is the gas constant ($8.314\ J\ K^{-1}\ mol^{-1}$), and T is the thermodynamic temperature. Table 5 shows the diffusion coefficients of Ti and Fe in α-Fe, α-Ti and β-Ti at 1155 K [24]. This leads to the fact that the diffusion coefficient of Ti to α-Fe is much smaller than that of Fe diffusing to both α-Ti and β-Ti, and in addition the diffusion coefficient of Fe to β-Ti is much larger than that of Fe diffusing to α-Ti even at the same temperature. Thus, in combination of large solubility of Fe in β-Ti, Fe-contained β-Ti was formed at the Ti-rich zone.

Fig. 11 shows the results of shear tensile test for the joints with two different kinds of interface microstructure formed by the different probe lengths. Each tensile shear force showed almost the same value, because both of them fractured at the base metal of CP-Ti plate as shown in Fig. 12. These results demonstrate that the lap joints had sufficient strength. The high strength of the lap joint can be supposed to result from the microstructures of the lap joint interface, where Fe–Ti intermetallic phases are dispersed and mixed with β titanium at the following conditions; at the case of non-intermixed interface, Fe–Ti intermetallics did not form a monolithic compound layer, but a composite layer with β-Ti phase as well as very thin thickness of the layer with 50 to 100 nm, or at the case of intermixed interface, a lamellar structure in which very thin Fe–Ti intermetallic compound layer of about 50 nm in thickness and β-Ti layer of about 1 μm in thickness were alternately formed, though total thickness reached up to about 300 μm. The generation of intermetallic phases is ineluctable at the interfaces, but the intermetallic phases are dispersed and mixed with β titanium by the rotating probe. It's the key point for getting a high strength Ti/SPCC lap joint by FSW.

4. Conclusions

The dissimilar lap joining of commercially pure CP-Ti plate in 1.0 mm thickness and SPCC plate in 3.2 mm thickness were conducted by friction stir welding using the tools with different probe lengths from 0.8 to 1.2 mm for the purpose of controlling the joint interface microstructure, and thereby improving the mechanical properties of the dissimilar lap joints. The results can be summarized as follows.

(1) The sound joints with high tensile shear strength showing the base plate fracture of CP-Ti were only achieved with the probe lengths of 0.9 and 1.0 mm.
(2) The TEM bright field images and electron diffraction patterns revealed the two types of the interface microstructure that with the probe length of 0.9 mm, a non-intermixed type interface with a thin single interlayer of about 50 to 100 nm in thickness, composed of FeTi intermetallic compound and β-Ti phase was formed, and with the probe length of 1.0 mm, an intermixed interface with lamellar structure in

which a thin FeTi or FeTi + Fe_2Ti intermetallic compound layer of about 100 nm in thickness and a thin β-Ti layer of about 1 μm in thickness were alternately formed.

References

[1] Cacciamani G, Keyzer DJ, Ferro R, Klotz UE, Lacaze J, Wollants P. Critical evaluation of the Fe–Ni, Fe–Ti and Fe–Ni–Ti alloy systems. Intermetallics 2006;14:1312–25.

[2] Tomashchuk I, Sallamand P, Andrzejewski H, Grevey D. The formation of intermetallics in dissimilar Ti6Al4V/copper/AISI 316 L electron beam and Nd:YAG laser joints. Intermetallics 2011;19:1466–73.

[3] Wang T, Zhang BG, Chen GQ, Feng JC, Tang Q. Electron beam welding of Ti-15-3 titanium alloy to 304 stainless steel with copper interlayer sheet. Trans Non-Ferrous Met Soc China 2010;20:1829–34.

[4] Zhang BG, Wang T, Duan XH, Chen GQ, Feng JC. Temperature and stress fields in electron beam welded Ti-15-3 alloy to 304 stainless steel joint with copper interlayer sheet. Trans Nonferrous Met Soc China 2012;22:398–403.

[5] Shanmugarajan B, Padmanabham G. Fusion welding studies using laser on Ti-SS dissimilar combination. Opt Lasers Eng 2012;50:1621–7.

[6] Gao M, Mei SW, Wang ZM, Li XY, Zeng XY. Characterisation of laser welded dissimilar Ti/steel joint using Mg interlayer. Sci. Technol Weld Join 2012;17:269–76.

[7] Akbari Mousavi SAA, Farhadi Sartangi P. Experimental investigation of explosive welding of cp-titanium/AISI 304 stainless steel. Mater Des 2009;30:459–68.

[8] Kahraman N, Gulenc B, Findik F. Joining of titanium/stainless steel by explosive welding and effect on interface. J Mater Process Technol 2005;169:127–33.

[9] Kundu S, Chatterjee S. Interface microstructure and strength properties of diffusion bonded joints of titanium-Al interlayer-18Cr–8Ni stainless steel. Mater Sci Eng A 2010;527:2714–9.

[10] Elrefaey A, Tillmann W. Correlation between microstructure, mechanical properties, and brazing temperature of steel to titanium joint. J Alloys Compd 2009;487:639–45.

[11] Elrefaey A, Tillmann W. Solid state diffusion bonding of titanium to steel using a copper base alloy as interlayer. J Mater Process Tech 2009;209:2746–52.

[12] Akbarimousavi SAA, GohariKia M. Investigations on the mechanical properties and microstructure of dissimilar cp-titanium and AISI 316L austenitic stainless steel continuous friction welds. Mater Des 2011;32:3066–75.

[13] Dey HC, Ashfaq M, Bhaduri AK, Rao KP. Joining of titanium to 304L stainless steel by friction welding. J Mater Proc Technol 2009;209:5862–70.

[14] Lee WB, Jung SB. Effect of microstructure on mechanical properties of friction-welded joints between Ti and AISI 321 stainless steel. Mater Trans 2004;45:2805–11.

[15] Fazel-Najafabadi M, Kashani-Bozorg SF, Zarei-Hanzaki A. Joining of CP-Ti to 304 stainless steel using friction stir welding technique. Mater Des 2010;31:4800–7.

[16] Liao J, Yamamoto N, Liu H, Nakata K. Microstructure at friction stir lap joint interface of pure titanium and steel. Mater Lett 2010;64:2317–20.

[17] Fazel-Najafabadi M, Kashani-Bozorg SF, Zarei-Hanzaki A. Dissimilar lap joining of 304 stainless steel to CP-Ti employing friction stir welding. Mater Des 2011;32:1824–32.

[18] Gao Y, Nakata K. Microstructural characterization and mechanical properties of friction-stir-welded dissimilar lap joint of CP-Ti and steel. In: Proc of IJS-JW 2013, Osaka, Japan, 259–65.

[19] JIS Z 3136. Specimen dimensions and procedure for shear testing resistance spot and embossed projection welded joints. Japanese Standards Association; 1999.

[20] Fujii H, Sun YF, Kato H, Nakata K. Materials science and engineering a-structural materials properties microstructure and processing. Mater Sci Eng A 2010;527:3386–91.

[21] Liao J, Yamamoto N, Nakata K. Effect of dispersed intermetallic particles on microstructural evolution in the friction stir weld of a fine-grained magnesium alloy. Metal Mater Trans A 2009;40:2212–9.

[22] Kostka A, Coelho RS, DosSantos J, Pyzalla AR. Microstructure of friction stir welding of aluminium alloy to magnesium alloy. Scr Mater 2009;60:953–6.

[23] Syarif J, Kurniawan E, Sajuri Z, Omar MZ. Influence of iron on phase stability and corrosion resistance of Ti–15%Cr alloy. Sains Malaysiana 2013;42:1775–80.

[24] The Japan Institute of Metals and Materials. Metals data book. 3rd ed. Tokyo: Maruzen; 1995.